JOURNAL OF
biomaterials
applications

Biomaterials for Drug Delivery

Journal of Biomaterials Applications
2019, Vol. 33(9) 1214–1231

DOI: 10.1177/0885328219830823
journals.sagepub.com/home/jba
SAGE

Modifying release of poorly soluble active pharmaceutical ingredients with the amine functionalized SBA-16 type mesoporous materials

Barbara Jadach[1], Agnieszka Feliczak-Guzik[2], Izabela Nowak[2], Bartłomiej Milanowski[1], Hanna Piotrowska-Kempisty[3], Marek Murias[3] and Janina Lulek[1]

Abstract

SBA-16 and two modified SBA-16 type ordered mesoporous silica were used as the carriers for ibuprofen (anti-inflammatory drug) and furosemide (loop diuretic drug). Modification of the solid carrier was prepared with chitosan or N-3[(amino(poly-propylenoxy)]aminopropyltrimethoxysilane. The samples of carriers and carrier-drug loaded materials were characterized by X-ray diffraction, N_2 adsorption, Fourier-transform infrared spectroscopy, thermogravimetry, and differential scanning calorimetry. The release profiles of active pharmaceutical ingredients were performed in media with different pH in the USP 2 apparatus as well as in two biorelevant media (fasted state simulated gastric fluid and fasted state small intestinal fluid) in USP 4 apparatus. The loading of active substances into mesoporous materials was performed with modified immersion method. The maximum content of deposited drug in mesoporous material was close to 12.0 and 2.2 wt.% for ibuprofen and furosemide, respectively. After drug adsorption, the reduction of BET surface area, pore volume and pore diameter of non-modified and modified SBA-16 was observed, while the cubic arrays of siliceous matrix were well preserved. The release profiles of ibuprofen and furosemide loaded in mesoporous materials in media with different pH and biorelevant fasted state simulated gastric fluid and fasted state small intestinal fluid showed that the new SBA-16 type materials modify the release profiles of furosemide, increasing the dissolution rate of these substances in the medium at pH 1.2. The cytotoxicity of the materials and permeability of drugs after their loading on SBA-16 materials were evaluated on Caco-2 model. The results of our study showed that mesoporous materials did not exert cytotoxic effects and did not influence on the permeability of both active pharmaceutical ingredients in relation to pure substances.

Keywords

Ibuprofen, furosemide, SBA-16 type materials, dissolution, oral drug delivery

Introduction

Modern pharmaceutical technology tends to achieve the therapeutic effect and minimize adverse side effects of the drug substance. Therefore, many research centers involved in the development of therapeutic systems try to deliver the drug in the proper dose, at a specific location of the body and during defined time. For several years, more and more attention in biomedical research draws on ordered mesoporous silica materials containing nanoscale pores.[1–4] A drug with molecule size in the nanoscale can be incorporated into the material, and locally released in a controlled manner.

[1]Department of Pharmaceutical Technology, Poznan University of Medical Sciences, Poznań, Poland
[2]Faculty of Chemistry, Adam Mickiewicz University in Poznań, Poznan, Poland
[3]Department of Toxicology, Poznan University of Medical Sciences, Poznań, Poland

Corresponding author:
Barbara Jadach, Department of Pharmaceutical Technology, Poznan University of Medical Sciences, ul. Grunwaldzka 6, Poznań 60-780, Poland.
Email: bajadach@ump.edu.pl

Chemical modification of the silica walls is also possible and lead to increase in adsorption amount of some APIs (active pharmaceutical ingredients), including peptides, proteins and growth factors on ordered mesoporous silica materials.[5–8]

The SBA-16 material is synthesized using Pluronic F127 as structure directing agent. It has a regular structure (3D-*Im3m* symmetry) possessing large pore sizes and thick pore walls. The effect of synthesis conditions on the structure and textural properties of the SBA-16 was investigated by Feliczak-Guzik et al.[9] as well as by different research groups.[10,11] Also, adsorptive properties of SBA-16 have been examined already.[6,7,12–15]

Due to the increasing interest in mesoporous materials (MMs) with hexagonal symmetry as potential drug carriers (e.g. SBA-15), as well as limited data on these properties with respect to materials in the form of spheres occurring with a specific cubic structure, the pores of which have a large capacity[16,17] research over the pharmaceutical use of new SBA-16 type materials seems to be justified.

In our first publication,[9] we presented the results concerned the development of the synthesis procedure for two new SBA-16-type MMs containing amine groups. However, the presented study is focused on the assessment of the availability of these new hybrid MMs to modify the release profiles and permeability of two model APIs from II and IV group of biopharmaceutical classification system (BCS). Ibuprofen (IBU) and furosemide (FUR) were chosen as the model drugs. IBU (class II BCS) is a nonsteroidal anti-inflammatory drug widely used in the treatment of pain and inflammation in rheumatic diseases[18] while FUR (class IV BCS) is a loop diuretic used in the treatment of edema associated with heart failure,[19] and with renal and hepatic disorders.

Materials

Pluronic F127 was purchased from Sigma-Aldrich; HCl and tetraethyl orthosilicate (TEOS) from Fluka; N-3[(amino(polypropylenoxy)]aminopropyltrimethoxysilane (60–65 wt.% in amine terminated polypropylene oxide methanol solution) from ABCR; whereas chitosan from Polysciences. The model drug FUR (Sri Krishna Drugs Limited) and IBU (Hubei Granules-Biocause Pharmaceutical Co.) were a gift from Polpharma SA Pharmaceutical Works and were used as received. Ethanol (99.5%), dissolution media: 0.1 mol/L HCl concentrate, acetate buffer pH 4.5 concentrate, phosphoric buffer pH 7.4 concentrate were purchased from Avantor Performance Materials S.A. SIF Powder Original used for fasted state simulated gastric fluid (FaSSGF) and fasted state small intestinal fluid (FaSSIF) preparations was received from Biorelevant.com. Hank's Balanced Salt Solution (HBSS) was acquired from Sigma-Aldrich. Water was purified in the Millipore water-purification system. CellTiter-Glo® Luminescence Cell Viability Assay (G7571) and transparent membranes (PIHPO1250) were provided by Promega and Millipore respectively. Phenol red-free DMEM, fetal bovine serum (FBS), glutamine, penicillin, streptomycin, dimethyl sulfoxide (DMSO) were purchased from Sigma-Aldrich Co. Acetonitrile and phosphoric acid were obtained from J. T. Baker.

Methods

Fabrication of non-modified and modified SBA-16 mesoporous materials

SBA-16 MM and its modifications were synthesized according to the procedure described in our previous work.[9] Briefly, 8.0 g of Pluronic F127 (structure directing agent) were mixed with 77.6 g of water and 320.0 g of 2 M HCl and stirred for 60 min at room temperature (RT). Next, 33.6 g of TEOS were added and stirred for 1 h. Formed precipitate in liquid was kept in oven at 90°C for 24 h. The solid was recovered by filtration, followed by drying at RT. The template was then removed by calcination in air at 550°C for 6 h.

The modification of surface was made with chitosan or N-3[(amino(polypropylenoxy)]aminopropyltrimethoxysilane 60–65% in order to receive SBA-16/CHIT and SBA-16/NH2 materials, respectively. For this purpose, during the synthesis 0.48 g of chitosan or 0.96 g N-3[(amino(polypropylenoxy)]aminopropyltrimethoxysilane 60–65% was added to the mixture of Pluronic F127, water, HCl and TEOS and kept in oven for 24 h at 90°C. The white solid was recovered by filtration and extracted with mixture of ethanol: HCl (100:1) at 60°C for 16 h to remove surfactant. Next solids were filtrated, washed with purified water and ethanol and dried at 60°C for 12 h. Each of the three tested materials was prepared in two independent batches that were mixed before further investigation.

Drug loading

Loading of drugs into MMs was carried out by immersion method according to modified procedure described, e.g. by Horcajada et al.[20]

Two series of non-modified SBA-16 samples and four series of modified SBA-16 (100 mg, $n = 50$, where n is number of batches) samples were placed in ampoules filled with 5 mL ethanol solutions of FUR (10 mg/mL) or IBU (65 mg/mL). Loading was performed at RT under shaking with 600 r/min for 24 h. Then, the MM samples were filtered with filters of

45 μm pore size and dried at oven at 50°C for 24 h. The dried samples of each series were combined and gently mixed to produce six homogeneous large samples denoted as MM/FUR or MM/IBU. The levels of loaded APIs were determined in three sub-samples of each loaded MM. For this purpose, 5 mg of loaded materials (MM/IBU and MM/FUR) were extracted with 5 mL of ethanol and stirred for 24 h (600 r/min). After filtration, the drug content in ethanol solution was determined by UV-Vis spectrophotometric method ($\lambda = 221$ nm and $\lambda = 277$ nm for IBU and FUR, respectively).The level of API loaded into each type of MM was expressed as weight percent (w/w% ±SD). The calculated drugs loading was used in dissolution/release experiments as supposed initial IBU or FUR content. The effective uptakes of both APIs on MM were also determined by TGA method.

Physicochemical and morphological characterization of non-loaded and loaded mesoporous materials

In order to characterize textural/structural/surface properties of unloaded and loaded MMs, the following methods were used: X-ray diffraction (XRD), Fourier-transform infrared spectroscopy (FTIR), N_2 physisorption, thermogravimetric analysis (TGA), differential scanning calorimetry (DSC), scanning electron microscopy (SEM), and laser diffraction (DL).

XRD patterns were measured with a Bruker AXS D8 Advance diffractometer (CuKα radiation, $\lambda = 0.154$ nm) in two 2Θ ranges: 0.6–10° (small angle XRD (SXRD)) and 4–60° (wide angle XRD (WXRD)) with the step size of 0.02° or 0.05°, respectively.

Adsorption/desorption experiments using nitrogen as adsorbent were carried out at –196°C on an Autosorb-iQ, Quantachrome. Before each measurement samples were outgassed in vacuum at 300°C for 4 h for SBA-16 sample, at 120°C for 8 h for the SBA-16/CHIT, SBA-16/NH2 and MM/FUR samples, and at 50°C for 12 h for MM/IBU, respectively. The N_2 isotherms were used to determine the specific surface areas using the standard BET equation in the relative pressure (p/p_0) from 0.05 to 0.2 and the cross-sectional area of nitrogen molecule of 0.162 nm^2. Pore sizes were obtained from the N_2 adsorption branch, using the Barrett–Joyner–Halenda (BJH) method with the corrected Kelvin equation, i.e. KJS–BJH method at the maximum of pore size distribution.[21] Furthermore, the α-plot analysis was performed for all examined samples for the evaluation of the micropores volume. The single-point total pore volume was obtained from the amount adsorbed at $p/p_0 = 0.98$.

Fourier-transform infrared spectroscopy was conducted using an FTIR Bruker IFS 66v/S spectrometer, in the range from 4000 to 400 cm^{-1}. FTIR spectra of tablets obtained by pressing at a pressure of ~25 MPa of a mixture of 0.001 g of material with 0.2 g KBr.

The morphology and topography of MM particles were assessed on the basis of the images obtained with the aid of the scanning electron microscope EVO40, made by Zeiss AG. Samples of materials were attached to the camera table with conductive double-sided adhesive film, then sprayed with gold in the Bal-Tec SCD050 rotary atomizer. A 19 kV acceleration voltage was used for imaging.

The TGA and DSC analyses were carried out between 25 and 950°C by using STA 449 F3 Jupiter Thermal Analyzer Netzsch. Approximately 20.0 mg of samples were analyzed using a heating rate of 10°C/min, with a nitrogen atmosphere flow of 25 mL/min and an open alumina cell.

The particle size distribution of the examined materials was investigated using Mastersizer2000 apparatus. The particles were measured in water suspension (dilution 1:4000).

Particle size distribution was referred as Span value[22] and calculated as follows:

$$\text{Span} = [d(0.9) - d(0.1)]/d(0.5) \quad (1)$$

where d(0.9), d(0.5) and d(0.1) are the volume size diameters at 90%, 50% and 10% of the cumulative volume, respectively. The smaller Span value indicates the narrower size distribution.[22]

Drug dissolution/release study

In order to study the drug release from IBU and FUR-loaded MMs, the APIs-loaded powders were suspended in 0.1 mol/L HCl (pH 1.2); acetate buffer (pH 4.5) or phosphate buffer (pH 7.4). The dissolution study was performed by using the paddle apparatus (ERWEKA DT 60, Germany), at 70 r/min and 37 ± 0.5°C. Samples of loaded materials whose amount corresponded to 2 mg or 0.25 mg of IBU or FUR, respectively were introduced into 125 mL of suitable dissolution medium. 4 mL of medium samples were taken after following time: 5, 15, 30, 45, 60, 75, 90, 105 and 120 min and the withdrawn aliquots were replaced with fresh dissolution media. All samples were filtered with a 45 μm pore size membrane, and APIs concentrations were determined by validated spectrophotometric methods ($\lambda = 221$ nm for IBU in all pH; $\lambda = 277$ nm for FUR at pH 4.5 and 7.4 and $\lambda = 234$ nm for FUR at pH 1.2).

Additionally, the dissolution and release processes were investigated using on-line open loop semi-automated flow-through cell dissolution system (SOTAX AG, Switzerland) using method defined by Chapter 2.9.43 Apparent Dissolution described in the

Ph. Eur. 8.0.[23] The dissolution system consisted of: SOTAX MS 47 4-position media sector with air separation, SOTAX CE 7 smart unit with a set of 7 cells for powders, SOTAX CP 7-35 piston pump, reservoirs for the dissolution medium and double-beam UV-Vis spectrophotometer Nicolet Evolution 300 equipped with linear cell changer and set of flow-through (path length = 10 mm) (Thermo Electron Corporation, USA). Pure IBU (10 mg) and FUR (2 mg) samples, as well as samples of loaded materials whose amount corresponded to 10 mg of IBU or 2 mg of FUR were examined. The "open on-line" method was used: the flow of media was 4 mL/min and it was FaSSGF during first 30 min then changed on FaSSIF for the next 90 min of investigation. APIs concentrations were determined on-line every one minute of the test by validated spectrophotometric methods. All experiments in paddle or flow-through cell apparatus were prepared in triplicate and under sink condition.

Dissolution data were evaluated using DD-Solver software.

Assays with Caco-2 cell culture

The colon Caco-2 cancer cell line was purchased from the European Type Culture Collection. Caco-2 cell line was maintained in phenol red-free DMEM supplemented with 10% FBS, 2 mM glutamine, penicillin (100 U/mL), and streptomycin (0.1 mg/mL). Cells were cultivated under standard conditions at 37°C in a humidified atmosphere containing 5% CO_2 and 95% air. To investigate the effects of materials tested on cell viability, confluent stock cultures were detached using trypsin and seeded in 96-well plates at a density of 2×10^4 cells/well. They were allowed to attach overnight and 100 µL of materials tested suspensions (in HBSS) of 0.2–4.0 mg/mL were then added. The cells were incubated at 37°C and stirred at a speed of 25 r/min for 3 h. Cell viability was measured using CellTiter-Glo® Luminescence Cell Viability Assay (Promega, USA).

Bidirectional transport assay

For transport assay, the Caco-2 cells were seeded at 4×10^5 cells/cm^2 onto transparent membranes (Millipore), (pore size 0.4 µm, growth area 0.6 cm^2) in clusters of 12 wells (Falcon). The growth medium was changed three times a week until time of use. Permeability of test compounds was measured in the apical-to-basolateral (A–B) and basolateral-to-apical (B–A) directions at 37°C with moderate shaking (25 r/min). Before initiation and after the test of the transport studies, the trans epithelial electric resistance (TEER) was measured with Millicell ERS-2 Epithelial Volt-Ohm Meter. Only the cells with TEER values of >450 Ω were used for the assay. Permeability screening was routinely performed under iso-pH condition (pH 7.4) in both directions. HBSS buffer at pH 7.4 was used on the apical (AP) and basolateral (BL) side. Before the permeability experiments, the cell monolayers were rinsed twice with HBSS and equilibrated in the transport buffers under experimental conditions for 30 min. Samples 100 µL were taken from the receiver side at 15, 30, 45, 60, 90 and 120 min and replace with pH 7.4 fresh HBSS and run in triplicate.

FUR and IBU permeation across Caco-2 monolayers was studied from pre-dissolved APIs solutions (controls) and from loaded non-modified and modified SBA-16 type materials suspended in HBSS buffer. The concentration of loaded materials was 2 mg/mL and the concentration of the control solutions was intended to correspond to that obtained after dissolution of the dose contained in the SBA-16 microparticles and was 40 µg/mL and, 200 µg/mL for FUR and IBU, respectively.

Apparent permeability coefficients

Identification and quantification of FUR and IBU in permeability experiments was performed by HPLC method on Shimadzu system consisting of Shimadzu LC-10AT VP with spectrophotometric detector SPD-10A VP. The used mobile phases was the same that those described by Salonen et al.[24] and during determination of FUR ($\lambda = 277$ nm; retention time t_r= 4.860 min) consisted of acetonitrile and 80 mM phosphoric acid (40:60 v/v) while during IBU determination ($\lambda = 221$ nm; retention time t_r= 4.302 min), of acetonitrile and 3 mM phosphoric acid (50:50 v/v). A Bianacom Velocity LPH C18, 3.0 × 150 mm, 3 µm (Bianacom) column was applied with mobile phase flow rates of 0.8 mL/min and 0.4 ml/min for IBU and FUR, respectively. The volume of injection was 20 µL.

Cumulative amounts of drugs transported across Caco-2 cell monolayers were calculated from APIs concentrations determined in the receiver compartments: basolateral compartment in A/B direction and apical compartment in B/A direction. Apparent permeability coefficients, P_{app} (cm/s), were calculated using the following equation:

$$P_{app} = DQ/DT * (1/A * C_0) \quad (2)$$

where DQ/DT is the flux of API across the monolayers (µg/min), A is the surface area of the cell monolayer (cm^2), and C_0 is the initial concentration (µg/mL) of the examined compound in the donor compartment. Results reported are mean P_{app} (cm/s) values ± SD ($n = 3$) based on data obtained up to 120 min.

Results and discussion

Characterization of the material before and after loading process

Morphology of SBA-16 type MMs in literature is described as irregular agglomerated particles.[13,25] All materials investigated in our study showed spherical morphology (Figure 1) with the tendency to agglomeration.

This agglomeration effect was also confirmed by DL technique examined with Mastersizer 2000 apparatus. The particle size distribution of SBA-16 and modified MMs both before and after drugs loading is shown in Figure 2 and reported in Table 1.

The particle size distribution depends on conditions during synthesis of the material. As shown in Figure 2, bi-modal particle size distribution is observed for all materials studied. Usually, non-modal distribution is typical for synthetic powders with hierarchic particles that form agglomerates with different sizes.[26] However, in our studies, these bi-modal particle size distributions could be because each type of MM was obtained in two independent batches that were mixed before characterization and loading with APIs. All three examined materials (before drug-loading) are composed of particles with similar particle sizes: 1–10 μm and 30–100 μm and a small fraction of particles with sizes higher than 100 μm.

For the samples SBA-16 and SBA-16/NH2 it is particularly evident that drug loading leads to a decrease of the left and an increase of the right peak of the particle size distribution (Figure 2(a) and (c)). This implies that e.g. a 5 μm particle is transformed to a 50 μm particle upon drug loading. It could this be due to agglomeration. Only for SBA-16/CHIT loading process did not cause big change in particle size distribution. The tendency for agglomeration of the particles depends on the structure of the material. Span values (Table 1) indicate not narrow particle size distribution. However span values for all used materials did not significantly change after adsorption of both APIs.

X-ray diffraction is the basic technique used to characterize MMs. The small-angle X-ray diffraction (SXRD) is an important source of information about the structure of nanometer sized materials. It allows to track phase transitions occurring on the surface. The SXRD patterns (Figure 3) for MMs before loading with APIs were in good agreement with references data of corresponding materials. All diffraction patterns for materials with the structure of the SBA-16 are characterized by having a single, intense reflection at an angle of $2\theta \approx 1°$.[15,27] The SXRD patterns for loaded materials also showed the reflections that correspond to SBA-16 structure but with lower intensity confirming that the adsorption process does not change the structure of materials with cubic symmetry and drugs have been incorporated inside the pores.[28]

The presence of signals in the wide-angle range (WXRD) confirms the presence of a substance in the crystalline form. Well-defined diffraction patterns in wide-angle scattering range indicate that the adsorbed drugs in MMs are crystalline, while the lack of signals characteristic of the crystalline structure of the APIs indicates a change of crystal phase these substances when combined with MM in amorphous form and loaded within the pores of MM.[13] As it was showed (Figure 4) examined APIs-loaded in the MMs seemed to be no longer in crystalline form.

Pure IBU and FUR showed intense and characteristic diffraction peaks that confirmed crystalline character of these substances (Figure 4, black line). SBA-16, SBA-16/CHIT, and SBA-16/NH2 before loading process showed no diffraction peaks (not shown here) due to their amorphous nature.[14] After incorporation of FUR and IBU into MMs, the characteristic peaks of crystalline FUR and IBU were not observed, that might confirm the non-crystalline state of APIs loaded in MMs. These results are in accordance with

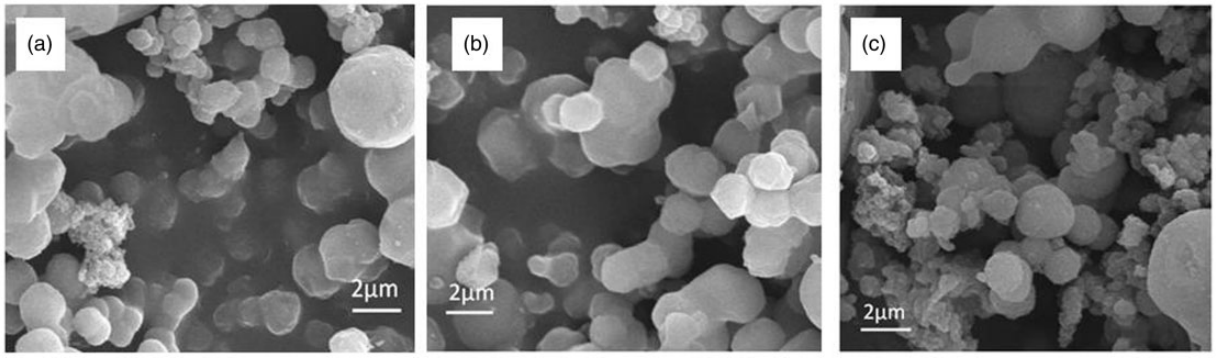

Figure 1. SEM images of mesoporous materials: (a) SBA-16, (b) SBA-16/CHIT and (c) SBA-16/NH2.
SEM: scanning electron microscopy.

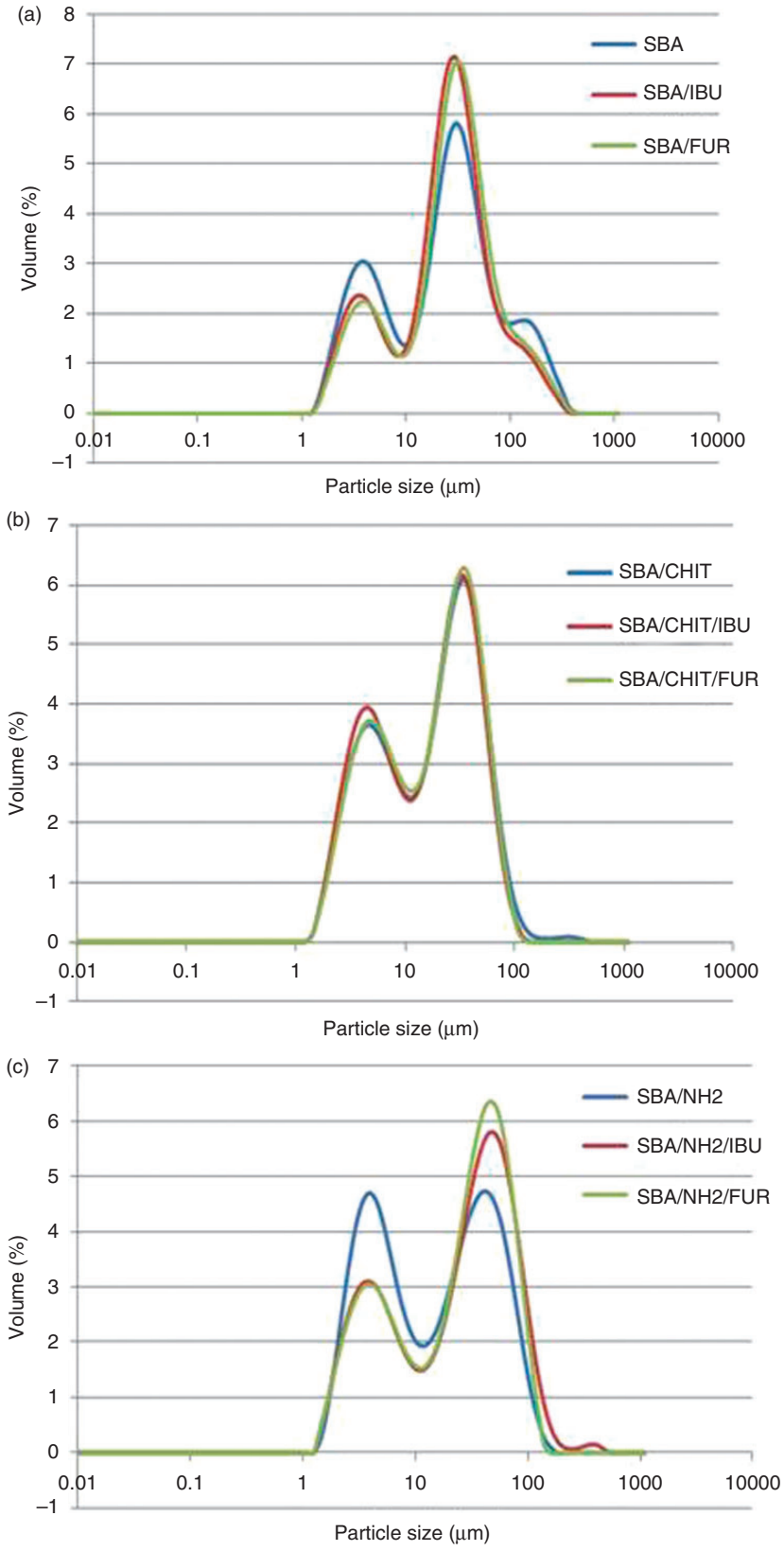

Figure 2. The influence of IBU or FUR loading on particle size distribution of mesoporous materials (a) SBA-16, (b) SBA-16/CHIT and (c) SBA-16/NH2.
IBU: ibuprofen; FUR: furosemide.

Table 1. Characterization of unloaded and IBU or FUR loaded SBA-16 and modified SBA-16 materials using different analytical methods.

	N_2 adsorption/desorption			APIs load (%w/w)		Particle size distribution				
Sample	S_{BET} (m^2/g)	V_P (cm^3/g)	D_P (nm)	UV-Vis	TG	d (0.1) (μm)	d (0.5) (μm)	d (0.9) (μm)	D (4.3) (μm)	Span
SBA-16	690	0.52	6.00	–	–	3.44	27.54	129.94	47.68	4.59
SBA-16/IBU	430	0.34	6.00	9.55±0.15	6.52	3.80	27.71	89.61	40.69	3.10
SBA-16/FUR	640	0.48	6.00	1.47±0.10	1.17	4.11	30.64	100.56	45.13	3.15
SBA-16/CHIT	350	0.31	6.64	–	–	3.58	21.27	60.08	28.24	2.66
SBA-16/CHIT/IBU	190	0.21	6.32	8.99±0.58	7.67	3.43	19.52	54.93	24.78	2.64
SBA-16/CHIT/FUR	230	0.23	5.75	2.29±0.04	0.98	3.63	20.67	56.51	25.68	2.56
SBA-16/NH2	330	0.36	6.24	–	–	3.05	16.95	69.54	28.00	3.92
SBA-16/NH2/IBU	140	0.20	5.72	11.57±1.60	5.34	3.25	30.77	89.08	40.46	2.79
SBA-16/NH2/FUR	230	0.27	5.88	2.47±0.08	2.00	3.30	30.26	79.19	35.62	2.51

IBU: ibuprofen; FUR: furosemide; APIs: active pharmaceutical ingredients; TG: thermogravimetry; S_{BET}: BET surface area; V_P: pore volume; D_P: pore diameter; d(0.1) (μm): 10% of the particle distribution is below this value; d(0.5) (μm): median of particle distribution (50% of the distribution above this value and 50% below); d(0.9) (μm): 90% of the particle distribution is below this value; D(4.3): the mean diameter over volume also called the de Broukere mean diameter; Span: the relative width of the distribution, calculated from formula: [d(0.9)-d(0.1)]/d(0.5)].

the results of other groups' works that investigated SBA-16 materials: different APIs after loading into SBA-16 were no longer crystalline.[7,13,14]

Nevertheless, it should be taken into account that small amounts of APIs loaded to MMs could not be detectable in XRD analysis.

Further observations of changes in the crystalline form of APIs were investigated with DSC analysis. If the API is located on the surface of the MM and is in crystalline form then sharp peaks correspond to melting temperature of API in the DSC curves will be observed.[29,30] If the material is in amorphous form, no peaks corresponding to melting endotherm peak will be detected in the DSC thermograms.[30] DSC curves of the pure crystalline IBU showed one endothermic pick at 74°C (Figure 5(a)) that corresponds to melting temperature of IBU. On DSC curve of crystalline FUR Tg point at 131–137°C was observed than at 214°C endothermic pick and further at 220°C exothermic pick (Figure 5(b)) that correspond to melting point and decomposition of FUR, respectively. DSC curves for materials loaded with IBU showed small rounded picks assigned to melting temperature of IBU (Figure 5 (a)), which may suggest that the IBU is within the pores in an amorphous form.[24,29,30] For materials loaded with FUR exothermic picks around the 220°C were not observed (Figure 5(b)), that can confirm that FUR inside the pores of the material is in the amorphous form.[29]

Hu et al. suggested that limited nanospace (voids) of MMs prevents the crystallization of APIs inside the pores.[13] Described in the literature studies with different MMs showed that crystalline form of FUR loaded in the SBA-15[30] or MCM-41[31] materials with hexagonal symmetry also change the form into non-crystalline. Heikkilä et al. reported similar results for IBU loaded in MCM-41, SBA-15 or TUD-1.[32] The authors have observed only one peak for IBU loaded in MCM-41 only when high loaded samples were prepared.

Unfortunately, as in the case of XRD, it should be taken into consideration the low sensitivity of the DSC method, bearing in mind the amount of IBU and FUR loaded into the tested MMs.

The successful drug loading characteristics of all investigated materials were confirmed by the results of nitrogen adsorption measurement. Figure 6 displays the nitrogen adsorption-desorption isotherms of MMs before loading (black lines) and after loading with IBU and FUR (red and blue lines, respectively). SBA-16 type materials exhibit type IVa isotherms[15,27,33] and the hysteresis loops of H2 shape ascribed to cage-like materials.[9,10,15]

The surface areas, pore sizes and pore volumes of investigated materials are listed in Table 1. The SBA-16 materials exhibit a bimodal pore size distribution (not presented here), which corresponds to the size of cages and the pores interconnecting them.[15] The nitrogen sorption isotherms of loaded with APIs materials showed noticeable decrease in the total volume of adsorbed nitrogen compared to silica materials before loading process. The volume of adsorbed nitrogen after modification of the structure was lower than for the unmodified material. After loading of APIs further changes in surface area, pore size and volume were observed. The adsorption of both drugs (IBU and FUR) in different materials lead to a decrease in pore volumes, surface area and pore diameter (Table 1) as in the studies, e.g. Hu et al.[14] and Otsuka et al.[34] This could be explained by the fact that APIs were located

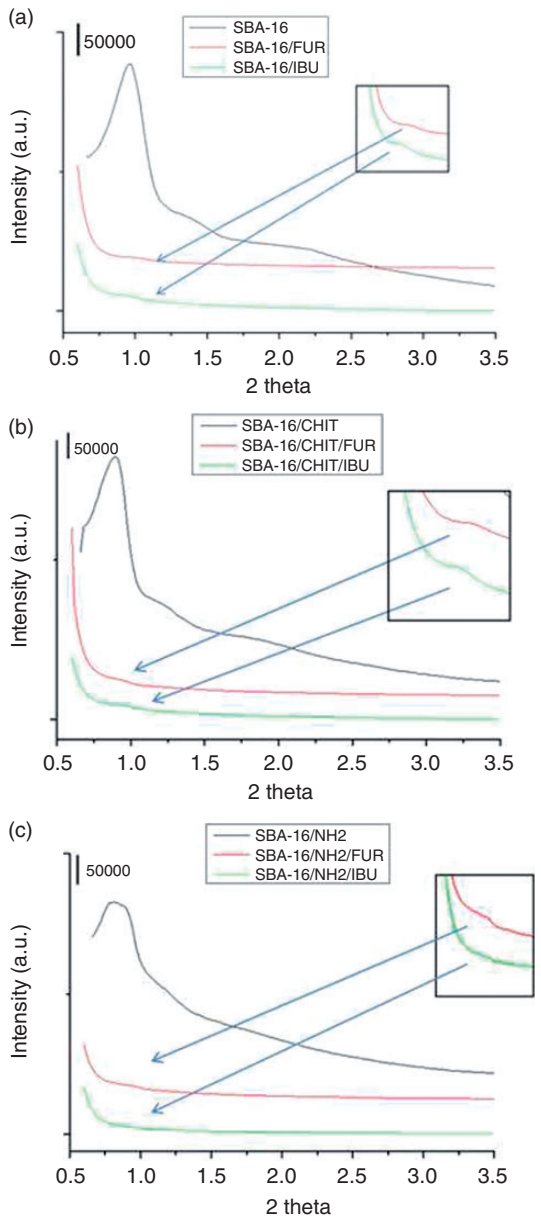

Figure 3. SXRD (small angle) patterns of mesoporous materials before and after loading FUR or IBU: (a) SBA-16, (b) SBA-16/CHIT and (c) SBA-16/NH2.
SXRD: small angle X-ray diffraction; FUR: furosemide; IBU: ibuprofen.

inside the pores and surface area was occupied with their molecules.[35,36]

The results obtained from FTIR spectra (400–1500 cm^{-1}) characterized the structure of mesoporous walls. All FTIR spectra (Figure 7) show the bands typical of mesoporous silica that were reported by the other authors.

The vibrational band at ~960 cm^{-1}, that is assigned to silanol group vibrational band ν(Si–OH) and it is characteristic for MMs.[7,37] The decrease of intensity of this band was observed after modification of SBA-16, and such a change is typically observed when the MM is modified.[7] For both examined SBA-16 type materials characteristic bands for silica materials are present: asymmetric vibrational band ν(Si–O–Si) from group SiO_4 at 1100–1050 cm^{-1} and band from SiO_4 vibrations at ~460 cm^{-1}.[10] The band at 3500 cm^{-1} is attributed to the silanol groups Si–OH that are present on the pore walls of the MMs.[35,38] In addition to bands characteristic of the inorganic part of the matrix, the vibrational bands corresponding to connections silicon-carbon ν(Si–C) at ~800 cm^{-1} in the spectra are also visible.[39,40] For all materials bands at 3000–2850 cm^{-1} corresponding to stretching vibration ν(C–H), bands at ~1640 cm^{-1} from stretching vibrational bands ν(C–C), at ~1455 cm^{-1} from symmetric deformation vibrations characteristic for carbon chain $\delta_s(CH_2)$ and at ~790 cm^{-1} for $(CH_2)_n$ also are present.

The APIs loaded MMs were characterized by FTIR to verify the presence of the functional groups after the drug adsorption. For all samples, after adsorption, all bands described above and assigned to silica materials were also observed. For materials loaded with IBU additional band was observed at 1704–1720 cm^{-1} corresponding to the ν(C–O) band that confirms the presence of this drug in the examined materials (Figure 7). Such a change was also observed by Horcajada et al. and Qu et al.[5,41] who incorporated IBU into different MMs. A band at 1516 cm^{-1} characteristic of aromatic ring system ν(C–C) present in the IBU structure was also observed. FTIR spectra of materials loaded with FUR, similar to those one reported by Ambrogi et al.,[35] showed bands characteristic of the sulfone group at ~1383 cm^{-1} and for the ν(C–Cl) band at ~578 cm^{-1} (Figure 7). The presence of all mentioned bands confirms that both drugs were introduced into MMs.

Drug loading and in vitro dissolution studies

In the next stage of our study, the influence of SBA-16 surface modification on the dissolution/release profiles of both model poor soluble APIs was evaluated.

Firstly, the amounts of APIs loaded into MMs was determined using two independent methods, it means ethanol extraction of adsorbates from MMs and by TG analysis. Quantification of IBU or FUR in ethanolic extracts was performed by UV-Vis method. The TG curves of unloaded and drug loaded MMs samples with a heating rate of 10°C/min were also investigated.[24,29,31] The loss of mass between melting temperature and decomposition temperature corresponded to the amount of API loaded on the MMs.[7,35] Use of the thermogravimetry in the quantification of the total

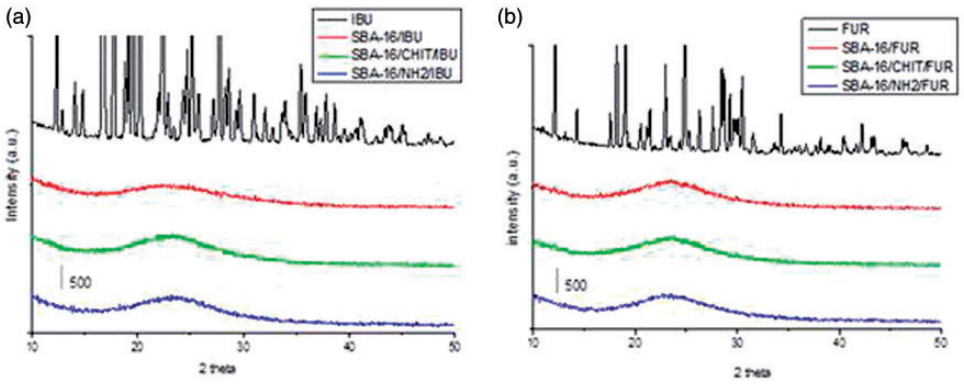

Figure 4. XRD (wide angle) patterns of: (a) IBU and (b) FUR in crystalline form and after loading on mesoporous materials.
XRD: X-ray diffraction; IBU: ibuprofen; FUR: furosemide.

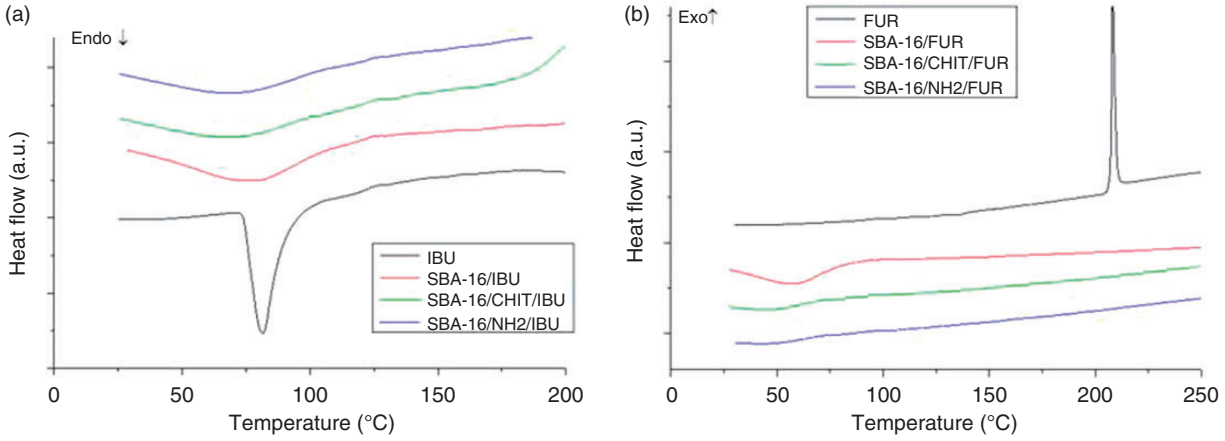

Figure 5. DSC curves of IBU (a) and FUR (b) in crystalline form and after loading on mesoporous materials.
DSC: differential scanning calorimetry; IBU: ibuprofen; FUR: furosemide.

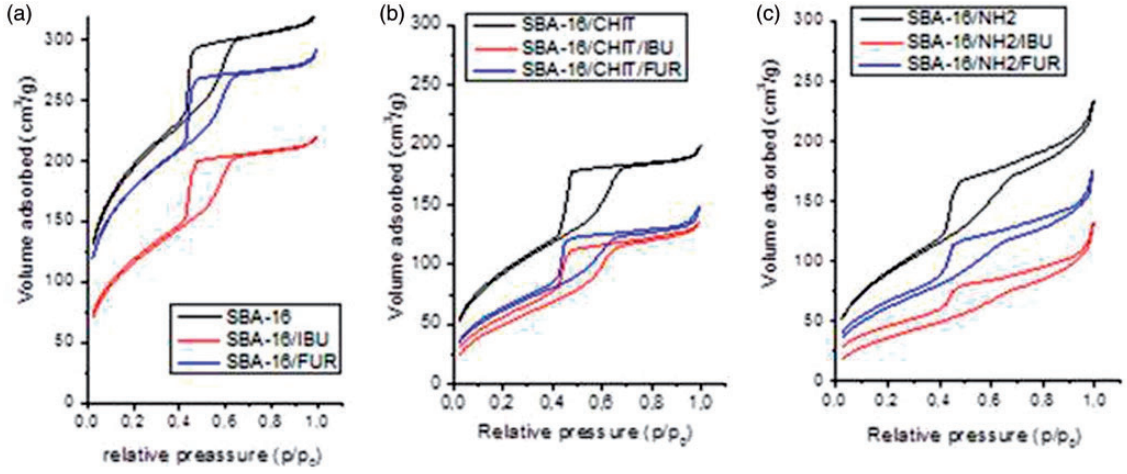

Figure 6. Nitrogen adsorption/desorption isotherms of (a) SBA-16, (b) SBA-16/CHIT, (c) SBA-16/NH2 before and after loading with IBU and FUR.
IBU: ibuprofen; FUR: furosemide.

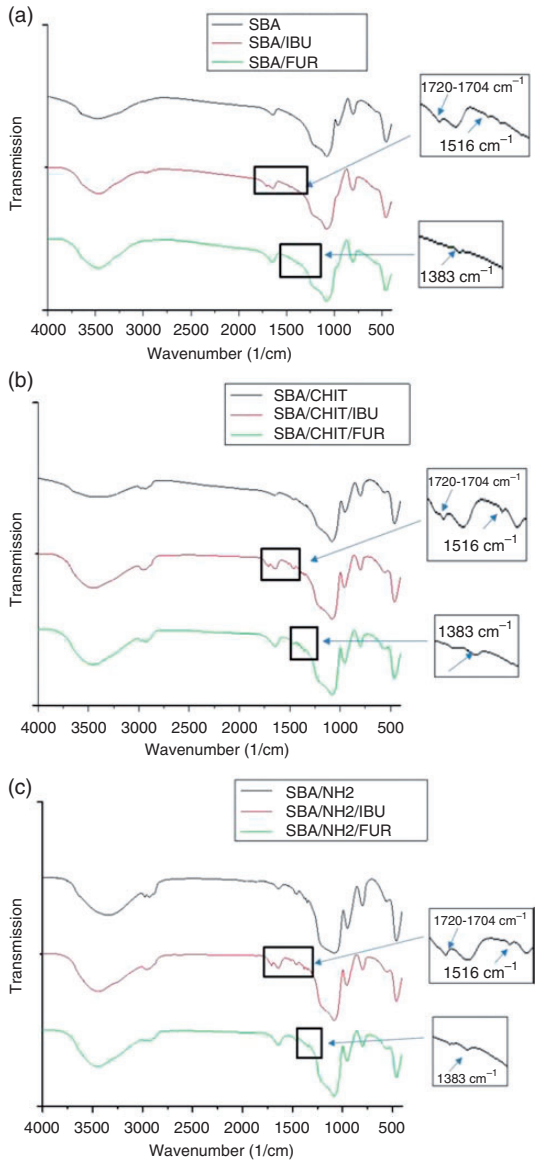

Figure 7. FTIR spectra of unloaded and IBU or FUR loaded (a) SBA-16, (b) SBA-16/CHIT, and (c) SBA-16/NH2.
FTIR: Fourier-transform infrared spectroscopy; IBU: ibuprofen; FUR: furosemide.

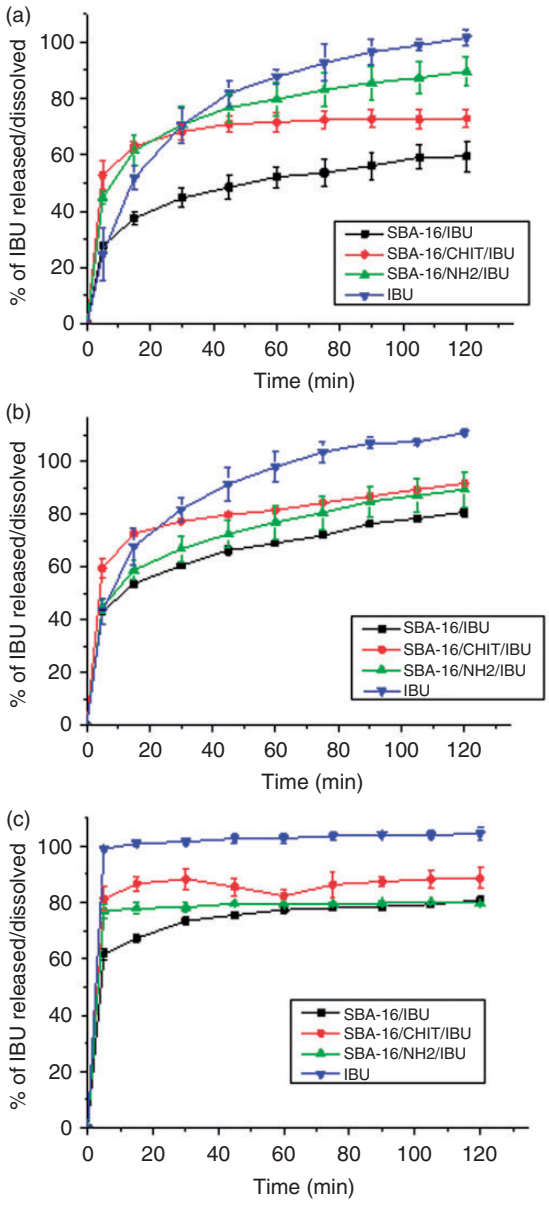

Figure 8. Effect of mesoporous materials composition on the dissolution/release profile of IBU determined by USP 2 method (paddle method) in: (a) 0.1 M HCl pH = 1.2, (b) acetate buffer pH 4.5 and (c) phosphate buffer pH 7.4. Results expressed as mean of three independent replicates (n = 3) ±SD.

drug content e.g. in MM sample is based on the fact that high enough temperature causes the organic compounds to decompose and desorb from the sample (figure not shown). Comparison of the mass decrease with the corresponding values obtained for pure drug and the unloaded porous matrix gives the total mass fraction of the drug.[31]

Considering that loading amounts of IBU and FUR determined with two independent techniques were different (Table 1), for release study the results obtained in extraction method was supposed as initial levels of API incorporated into examined MMs.

Analyzing the data presented in Figure 8 the pronounced effect of both unmodified and modified MMs on release profiles of IBU at all examined media can be seen. In the medium of pH 1.2 for the first 30 min, the release of IBU from MMs and its dissolution was faster than the dissolution of the pure substance itself (Figure 8(a)). After 30 min, the amount of dissolved crystalline IBU and IBU released from SBA-16/CHIT/IBU and SBA-16/NH2/IBU was approx. 70%, while release rate of adsorbate from modified MMs between 0 and 30 min was faster than

the dissolution rate of the crystalline API. After 60 min SBA-16/CHIT/IBU and SBA-16/NH2/IBU released 71 and 79% of IBU, respectively, while SBA-16/IBU released only 55% of API. Probably the interaction of IBU and non-modified material was stronger than between IBU and modified materials and in this way, the release of API from modified materials was faster. IBU release profiles at pH = 4.5 (Figure 8(b)) both SBA-16 and modified materials differ to the dissolution profile of the crystalline form of the drug. It was confirmed by the calculated values (<50) of the similarities factors f_2 (Table 2). After 60 min of the test 69–81% IBU loaded on MMs was released while at the same time 97% of crystalline API was dissolved. At pH 7.4 after 15 min release/dissolution of more than 70% IBU adsorbed on each of the MMs was observed (Figure 8 (c)) and the plateau on the release profiles at approx. 70–80% was reached. Reduced levels of IBU released/dissolved from the mesoporous carriers compared to the amount of the dissolved crystalline form of the drug (approx. 100% after 15 min) can be resulted from the stronger interaction of IBU-MM than IBU-medium or with restrictions in a casual diffusion of IBU inside the structure of MM.

Comparison of IBU and FUR dissolution and release profiles from all possible pairs of materials for media with different pH was performed by similarity factor f_2 method according to equation (3), using DDSolver software:

$$f_2 = 50*\log\left\{\left[1+\frac{1}{n}\sum_{t=1}^{n}(R_t - T_t)^2\right]^{-0,5}*100\right\} \quad (3)$$

where R_t and T_t are the percentage dissolved of the reference and test profile, respectively, at time point t and n is the number of sampling points.[42]

The FDA guidelines[42] suggest, that two profiles can be considered similar if f_2 is greater than 50 (50–100). The f_2 values obtained in our study are summarized in Tables 2 for IBU and FUR, respectively.

As shown in Table 2, at pH 1.2, the values of f_2 for IBU versus SBA-16/IBU, SBA-16/CHIT/IBU, and SBA-16/NH2/IBU as well as SBA-16/IBU versus SBA-16/CHIT/IBU, and SBA-16/NH2/IBU indicate lack of profiles similarity (f_2<50). It confirms the ability both SBA-16 and new SBA-16 type materials to modify the profile of dissolution/release of IBU – a model poorly soluble substance from the BCS Class II. It should be noted that the similarity of the profiles at pH 1.2 was found only for SBA-16/CHIT/IBU vs. SBA-16/NH2/IBU. These phenomena can be attributed to the introduction of amino groups into SBA-16

Table 2. Similarity factors f_2 values for IBU and FUR dissolution and release profiles for media with different pH (paddle apparatus). The values that indicate dissimilarity are bold-marked.

		Similarity factor f_2 value (profiles are similar when f_2 > 50)		
pH	Tested material	SBA-16/IBU	SBA-16/CHIT/IBU	SBA-16/NH2/IBU
1.2	IBU	**25.24**	**35.55**	**49.10**
	SBA-16/IBU	x	**35.72**	**29.56**
	SBA-16/CHIT/IBU	**35.72**	x	50.54
4.5	IBU	**30.96**	**41.56**	**32.73**
	SBA-16/IBU	x	**43.87**	58.08
	SBA-16/CHIT/IBU	**43.87**	x	55.03
7.4	IBU	**28.59**	**40.07**	**32.51**
	SBA-16/IBU	x	**43.36**	59.69
	SBA-16/CHIT/IBU	**43.36**	x	57.53
pH	Tested material	SBA-16/FUR	SBA-16/CHIT/FUR	SBA-16/NH2/FUR
1.2	FUR	**34.70**	**13.33**	**14.34**
	SBA-16/FUR	x	**23.40**	**25.06**
	SBA-16/CHIT/FUR	**23.40**	x	74.10
4.5	FUR	**18.93**	**11.70**	**11.97**
	SBA-16/FUR	x	**38.28**	**38.52**
	SBA-16/CHIT/FUR	**38.28**	x	86.72
7.4	FUR	**43.58**	**34.28**	**35.86**
	SBA-16/FUR	x	**48.16**	54.30
	SBA-16/CHIT/FUR	**48.16**	x	69.45

IBU: ibuprofen; FUR: furosemide.

Table 3. Similarity factors f_2 values of IBU and FUR dissolution/release profiles in simulated physiological conditions of the upper gastrointestinal in the fasted state, received in flow-through cell apparatus (FaSSGF pH = 1.6, 30 min; FaSSIF pH = 6.5, 30–90 min; the values that indicate dissimilarity are bold-marked).

	Similarity factor f_2 value (profiles are similar when $f_2 > 50$)		
Tested material	SBA-16/IBU	SBA-16/CHIT/IBU	SBA-16/NH2/IBU
IBU	**40.15**	**23.52**	**26.12**
SBA-16/IBU	X	**32.55**	**39.92**
SBA-16/CHIT/IBU	**32.55**	x	57.80
Tested material	SBA-16/FUR	SBA-16/CHIT/FUR	SBA-16/NH2/FUR
FUR	**31.35**	**22.53**	**18.36**
SBA-16/FUR	X	**39.61**	**35.11**
SBA-16/CHIT/FUR	**39.61**	x	**45.01**

IBU: ibuprofen; FUR: furosemide.; FaSSGF: fasted state simulated gastric fluid; FaSSIF: fasted state small intestinal fluid.

structure, both in the case of the SBA-16 surface modification by chitosan (SBA-16/CHIT) and by N-3[(amino(polypropylenoxy)]aminopropyltrimethoxysilane (SBA-16/NH2). The effect of the SBA-16 surface modification on IBU release profiles can be observed in the case of experiments performed using media at pH 4.5 and 7.4, respectively. Comparing the release profiles for unmodified and modified materials SBA-16 similarity of profiles were demonstrated for SBA-16/IBU and SBA-16/NH2/IBU as well as SBA-16/CHIT/IBU and SBA-16/NH2/IBU both pH 4.5 and 7.4.

A more pronounced effect of SBA-16 and its modified forms on the dissolution/release profile of the sparingly soluble API was found for FUR. The quantity of FUR released in 0.1 M HCl after 120 min of experiment increase twice from SBA-16 and more them six times from both new SBA-types materials. Crystalline FUR possesses pH-dependent solubility, after 120 min of the experiments we observed that the increased pH of the medium increases the percentage of dissolved FUR from approx. of 17% (medium pH 1.2) to approx. to 100% (medium pH 7.4). The dissolution study showed a pronounced effect of the mesoporous carrier on the release profiles of FUR in 0.1 M HCl (pH = 1.2) and acetate buffer pH 4.5 (Figure 9(a) and (b), Table 2). At lower pH (1.2 and 4.5) the significant increase in the dissolution/release rate of the drug from unmodified SBA-16 in comparison to pure API in the first 30 min of experiments were observed. An even greater effect was observed in the carrier materials modified with amino groups (Figure 9).

SBA-16/NH2/FUR and SBA-16/CHIT/FUR released after 120 min approx. 70% of the adsorbed FUR. It was almost more than double the amount of FUR released from the unmodified SBA-16 and almost four times more soluble than crystalline FUR at the same time in 0.1 M HCl. In studies using a medium at pH = 4.5 (Figure 9(b)) observed significantly higher levels of FUR released from MMs than the amount of crystalline form dissolved in the first 15 min of the experiment. At the same time, it was released more than 50% of FUR loaded in the SBA-16 and approx. 80% FUR adsorbed on the modified material, while the amount of dissolved crystal form of FUR does not exceed 8%. At pH 7.4 after 15 min release over 70% of FUR adsorbed on each of the modified MMs was observed. The approx. 10% more of the compound was released at the same time from SBA-16/FUR or dissolved from crystalline FUR (Figure 9(c)). Noteworthy achieve a similar level plateau in the case of the modified materials (70–75%) and slightly higher for SBA-16 (>80%). As in the case of IBU (Figure 8(c)) at pH = 7.4 after 120 min of the experiment was found the incomplete release of the adsorbate (FUR) both material SBA-16 and its modified forms (Figure 9(c)). It may result from improperly assumed starting amounts of adsorbate in the tested materials (Table 1). The output value of the load level MMs has been determined a priori, because of the variation in the degree of load MMs substances in model determined by various analytical techniques or, what seems to be more likely with a stronger impact than the MM-FUR FUR-medium and/or restrictions on the free diffusion FUR by MM structure. Complete dissolution of the crystalline forms of IBU or FUR after 15 and 120 min, respectively, were possible because of sink conditions during the whole experiment.

Our results are in good agreement with the results of Salonen et al. or Heikkilä et al.[24,30,32,43] who demonstrated that the incorporation of FUR into a MMs TCPSi tends to improve its release *in vitro* at lower pH. Also, Ambrogi et al. studying FUR loaded into

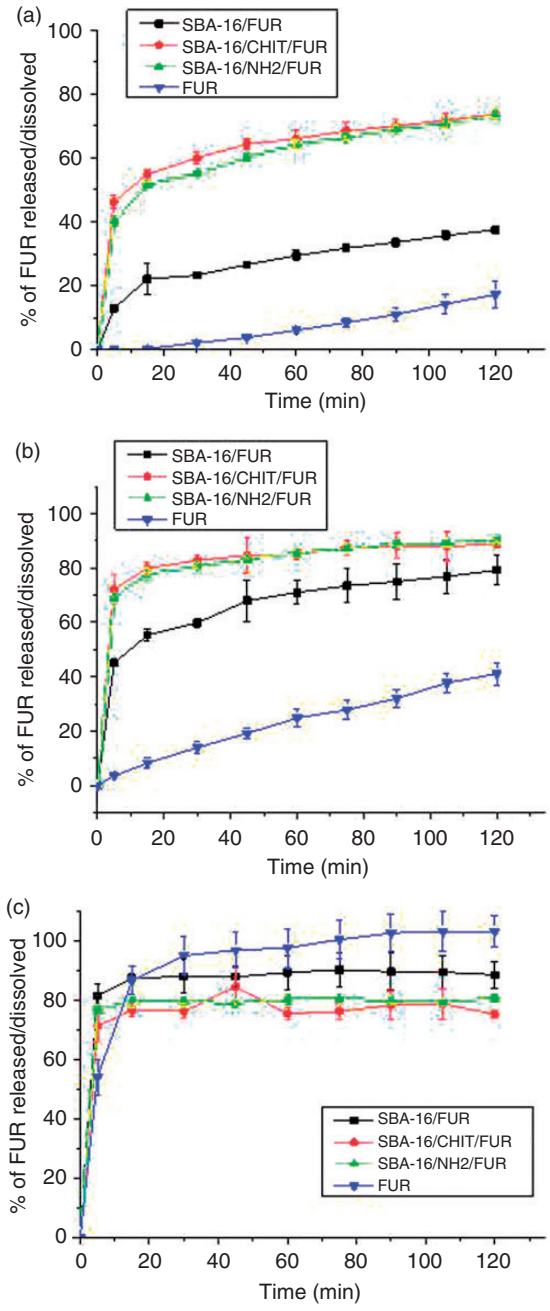

Figure 9. Effect of mesoporous materials composition on the dissolution/release profile of FUR determined by USP 2 method (paddle method) in: (a) 0.1 M HCl pH = 1.2, (b) acetate buffer pH 4.5 and (c) phosphate buffer pH 7.4. Results expressed as mean of three independent replicates (n = 3) ±SD.
FUR: furosemide.

MCM-41 or SBA-15 materials[35,38] have been obtained the better dissolution of FUR loaded on MMs than crystalline FUR itself. The acidic nature of FUR is demonstrated in its increased dissolution at higher pH-values. Furosemide molecules are not ionized at pH 1.2 (pH<pKa) and therefore most of the FUR molecules are in a stationary phase. Hydrogen bonding between FUR and SBA-16 is relatively weak, so the diffusion of FUR molecules through the channels will be the controlling step, such that the release is faster for FUR loaded into MM than for its crystalline form. As the solubility depends on the degree of crystallinity of a given substance, the assumed amorphous form of FUR in MM may be responsible for the faster dissolution of the drug.

As in the case, IBU designated values of coefficients f_2 indicate a lack of similarity between the dissolution profile of the crystalline FUR and the release profiles of this drug from MM/API systems in each of the tested media (Table 2). This indicates the ability of examined materials to modify the release profile of sparingly soluble substances, e.g. from the BCS class IV. Modification of the structure of SBA-16 with chitosan significantly affects the release rate of FUR. It should be noted that the lack of the similarity of the profiles obtained at all pH was found for SBA-16/FUR vs. SBA-16/CHIT/FUR. The similarity of profiles was found only for materials SBA-16/NH2/FUR vs. SBA-16/CHIT/FUR regardless of the pH of the medium used, and additionally at pH = 7.4 for SBA-16/FUR vs. SBA-16/NH2/FUR. For none of the tested media, there was no similarity between the FUR profiles from unmodified and modified SBA-16 materials (f_2<50). Similarly, to the IBU results, the similarity in FUR release (f_2>50) was only found in the profiles obtained for modified MMs (SBA-16/CHIT and SBA-16/NH2).

The above results (Figures 8 and 9, Table 2) suggest that introducing amino groups into SBA-16 using various modifying agents (chitosan and N-3[(amino(polypropylenoxy)]aminopropyltrimethoxysilane) leads to new ordered MMs with similar properties and confirm their ability to modify the release profiles of poorly soluble APIs. It was also found that the surface modification of SBA-16 by the introduction of amino groups clearly affects to increase the release rate and released the amount of FUR comparing to these obtained with the unmodified form of MM. Particularly well this is evident in the case of dissolution and releases studies of FUR at pH = 1.2 (Figure 9(a)).

Dissolution of both APIs under simulated physiological conditions of the upper gastrointestinal in the fasted state was also investigated. Flow apparatus equipped with powder cells in open on-line configuration was used for this evaluation. Profiles of the apparent dissolution rate of crystalline forms of IBU and FUR and the release profiles of APIs adsorbed on MMs SBA-16, SBA- 16/CHIT, SBA-16/NH2 are presented in Figure 10.

The similarity of the dissolution curves was analyzed by an independent model, based on a comparison of the similarity factor f_2.[44,45] Comparison of IBU profiles

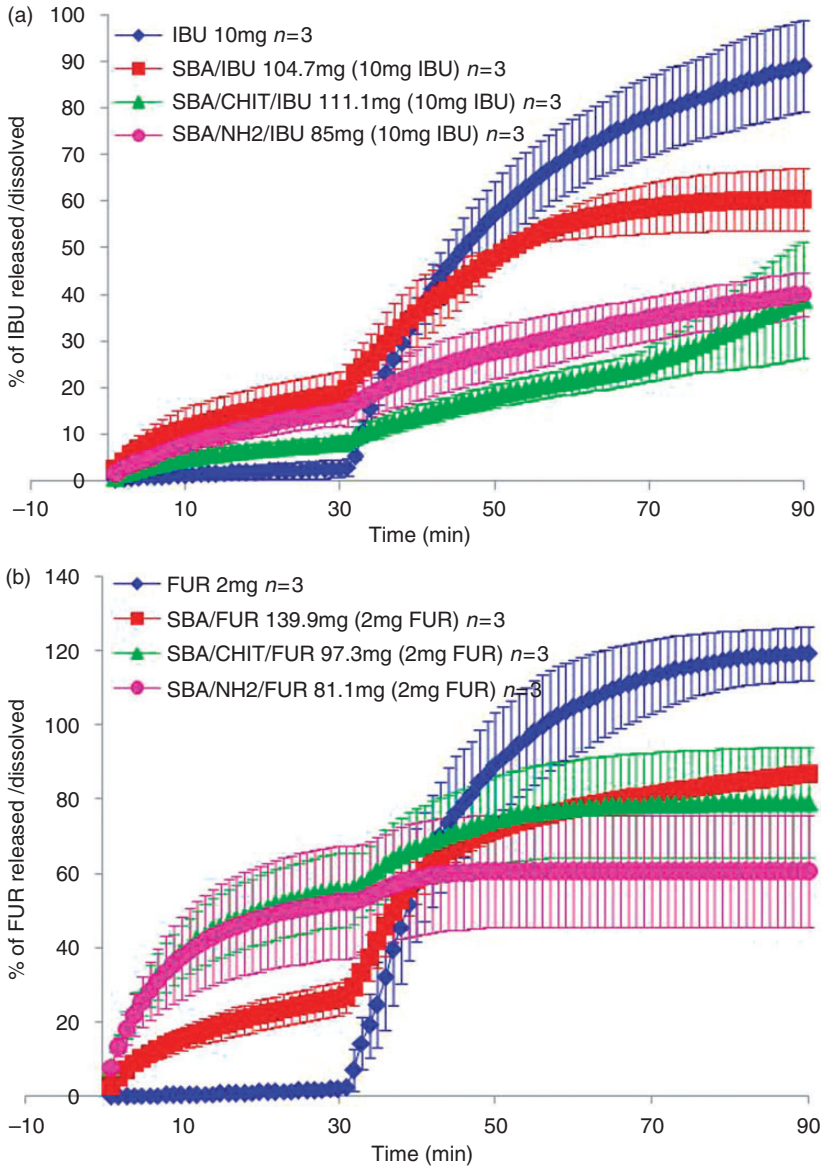

Figure 10. Effect of mesoporous materials on the dissolution rate of: (a) IBU or (b) FUR determined by USP 4 method (flow-through cell method) in FaSSGF and FaSSIF.
IBU: ibuprofen; FUR: furosemide; FaSSGF: fasted state simulated gastric fluid; FaSSIF: fasted state small intestinal fluid.

(Table 3, Figure 10(a)) by the similarity coefficients f_2 showed the only similarity between SBA/CHIT/IBU and SBA/NH2/IBU curves. On the other hand, in the case of FUR, dissimilarity of the dissolution profile of the active substance from all tested materials was observed (Table 3, Figure 10(b)).

Analysis of the amount of dissolved API in simulated conditions found in the stomach in the fasted state (FaSSGF, pH = 1.6; 30 min) showed a 3–7-fold more IBU released from MM compared to the dissolved amount of the crystalline material, and up to 14–30 times higher amounts of FUR released from MM vs. crystalline FUR. This confirms the results of a number of authors that the incorporation of API in silica MMs increases the rate and amount of active substance dissolved in pH <pKa.[30,38] This is the result of amorphization of API inside the pores, increase of surface wettability and dissolution and weak interactions (hydrogen bonding) between drug and MM. Specific increase rate was observed for modified SBA-16/NH2/FUR and SBA-16/CHIT/FUR (Figure 10(b)). Twofold greater amount of FUR released during first 30 min to FaSSGF was observed compared to the unmodified material SBA-16/FUR due to the presence and interaction of the organic groups of FUR in an acidic environment (excess protons). Concentrations of FUR released

to FaSSGF from the modified MM in the first minutes of the test indicate the formation of a supersaturated solution (concentration of the saturated solution of FUR in FaSSGF is 14 mg/L).[34] Tsume et al. recently proposed[46] introduction of the BCS system subclasses for classes of poorly soluble compounds of a weak acid. According to them, IBU was classified in class IIa and FUR into class IVa. The low pH prevailing in the stomach is not conducive to their ionization and dissolution, and increased the pH of the small intestine improves the solubility to allow quick passage of the solution, as for the substance class I. The absorption rate is so in this case limited by the rate of gastric emptying and increasing in the remaining segments of the small intestine due to the increase of pH in the light of these. This is particularly important in the case of drugs with so called absorption window (FUR is absorbed in the proximal part of the small intestine)[19] so that the observed phenomenon of the supersaturation during release of FUR from the FUR-modified MM in the simulated gastric fluid can affect the rate of drug absorption and bioavailability.

In turn, after 30 min when the fluid was changed from FaSSGF to FaSSIF drastic increase in the rate of dissolution of crystalline forms IBU and FUR (Figure 10) was observed. These results from a change in pH from 1.6 to 6.5 and increased ionization of drug molecules in the simulated small intestine environment. At the same time, slower changes in the amount of released IBU and FUR from MM in the simulated intestinal fluid in the fasted state as compared to the crystalline API were observed (82% of IBU dissolved in 90 min and >100% of the dissolved FUR at 70 min of the assay).

For IBU slower release from the MM modified was observed compared to the starting SBA-16 (Figure 10 (b)), suggesting a strong interaction with the drug molecules with organic groups inside the mesopores in simulated intestinal fluid environment fasting (controlled release mechanism).

Cytotoxicity and permeability – Investigation on Caco-2 cell line

Our results showed that the tested material SBA-16, as well as its modified forms (SBA-16/NH2 and SBA-16/CHIT) did not exert cytotoxic effects against human colon cancer cells Caco-2 (Figure 11) except for the highest material concentration used (4 mg/mL). Our findings are in accordance with the results of studies conducted by Andrade et al.,[7] although, they used MTT test for the cytotoxicity examination.

Human colon cancer cell line Caco-2 was also used in the permeation study. The integrity of the Caco-2 monolayers was ensured prior to use in the experiments by measuring the TEER-values before and after pre-equilibration in transport buffer. The resistance of the monolayers used was quite consistent, with the value >450 Ω cm^2 at the start of the experiment. The TEER values decreased in all experiments but did not drop below 250 Ω cm^2 and the lowest value measured was 336 Ω cm^2 after a pH 7.4 solution experiment. Permeability assay showed that both pure IBU and IBU loaded on MMs had permeability coefficient $P_{app} > 10 \times 10^{-6}$ cm/s, which corresponds to substances with good permeability (Table 4). Our results are in agreement with other authors' findings that IBU is classified into II BCS class.[47]

The differences in P_{app} were observed in both directions. The loaded materials showed smaller P_{app} values and the differences were 17–28% for A/B direction and 5–25% for B/A one. These changes do not influence the classification of IBU in BCS.

After introducing IBU and FUR into mesoporous carriers no significant changes in the P_{app} parameter values were noted. From point of view of penetration through biological membranes, it can be suggested that

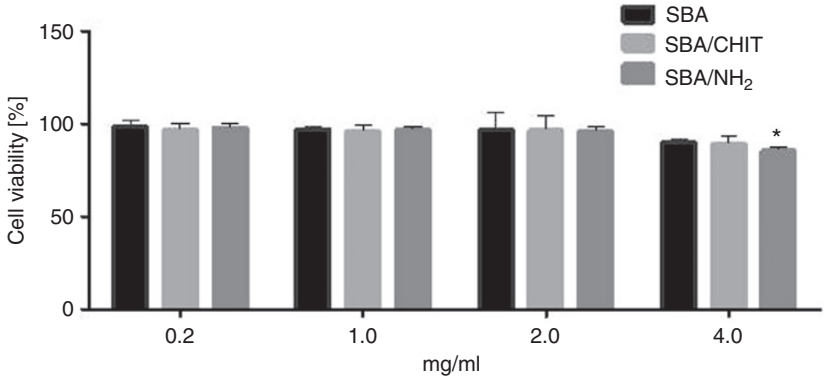

Figure 11. Cytotoxicity of SBA-16 and SBA-16 type materials in Caco-2 cell culture model. Results expressed as mean of three independent replicates ± SD.

Table 4. Permeability coefficients of ibuprofen (IBU) and furosemide (FUR) itself and incorporated into mesoporous carriers, determined with Caco-2 monolayers (pH 7.4; n = 3).

Sample	$P_{app} \times 10^{-6}$(cm/s)	
	Apical-to-basolateral transport	Basolateral-to-apical transport
IBU	50.6 ± 3.3	40.7 ± 4.5
SBA-16/IBU	37.9 ± 8.0	33.3 ± 3.9
SBA-16/CHIT/IBU	41.7 ± 3.7	30.4 ± 3.9
SBA-16/NH2/IBU	36.6 ± 2.3	38.5 ± 2.0
FUR	1.2 ± 0.3	10.10 ± 5.0
SBA-16/FUR	3.5 ± 1.8	8.1 ± 2.4
SBA/16/CHIT/FUR	2.2 ± 0.8	11.2 ± 1.3
SBA-16/NH2/FUR	2.1 ± 1.1	7.4 ± 1.2

the used carriers are unlikely to change the IBU bioavailability.

Our results confirmed low permeability of FUR itself ($P_{app} < 8 \times 10^{-6}$ cm/s).[19,48,49] Observed differences in A/B and B/A directions were in good agreement with the data presented by Granero et al.[19] When FUR was loaded into SBA-16 type materials, its permeability coefficient increased 2–3 folds for A/B direction, while for B/A direction we observed 10% increase of P_{app} only for FUR loaded on SBA-16/CHIT. The values of P_{app} coefficients for FUR loaded on SBA-16 and SBA-16/NH2 decreased by 17 and 27%, respectively. All observed changes do not influence the classification of FUR into low permeability class.

Conclusions

Surface modification of SBA-16 by the introduction of amino groups and chitosan influences the release profile both IBU and FUR. The influence of new materials on modifying the release profile of sparingly soluble FUR is particularly evident in the medium at pH 1.2. A significant increase in the FUR release/dissolution rate may result in an increase its bioavailability from solid dosage forms administered by the oral route.

The levels (>90%) of survival cell line Caco-2 exposed to increasing amounts of unmodified SBA-16 and its modified forms indicate negligible cytotoxicity of all examined materials, which is very important from the point of view of their future applications as carriers modifying the release of poorly soluble drugs.

The absence of significant differences in the permeability coefficients values of both IBU and FUR incorporated in the MMs in comparison to itself APIs, in the Caco-2 model suggests, that the application of new carriers will neither affect the permeability of IBU nor improve the permeability of FUR.

Considering the presented characteristics of SBA-16 and modified SBA-16 type materials, its influence on IBU and FUR release profiles in media at different pH, and under conditions simulating the various sections of the gastrointestinal tract, as well as negligible cytotoxicity evaluated MMs there are reasonable grounds for further development of these materials as potential carriers modifying the release of poorly soluble APIs. Further research should include, (i) optimization of the conditions incorporating active ingredients required to obtain such levels of API in the carrier, which both correspond to therapeutic doses of the drug and on the other would allow the development of pharmaceutical forms, (ii) refine synthetic procedures MM and the way of incorporating the API for the possibility of scaling both processes, and (iii) determining the stability of the active substance incorporated in the mesoporous carriers.

Acknowledgements

The authors acknowledge Polpharma SA Pharmaceutical Works (Starogard Gdański, Poland) for supplying the ibuprofen and furosemide used in this study.

Declaration of Conflicting Interests

The author(s) declared no potential conflicts of interest with respect to the research, authorship, and/or publication of this article.

Funding

The author(s) disclosed receipt of the following financial support for the research, authorship, and/or publication of this article: This study was supported by NN405667840 grant of the National Science Center (Poland).

ORCID iD

Barbara Jadach http://orcid.org/0000-0001-5222-4557
Bartłomiej Milanowski http://orcid.org/0000-0002-6450-174X

References

1. Vallet-Regí M, Balas F and Arcos D. Mesoporous materials for drug delivery. *Angew Chem Int Ed Engl* 2007; 46: 7548–7558.
2. Vallet-Regi M, Balas F, Colilla M, et al. Drug confinement and delivery in ceramic implants. *Drug Metab Lett* 2007; 1: 37–40.
3. Vallet-Regí M, Ruiz-González L, Izquierdo-Barba I, et al. Revisiting silica based ordered mesoporous materials: medical applications. *J Mater Chem* 2006; 16: 26–31.
4. Wang S. Ordered mesoporous materials for drug delivery. *Micropor Mesopor Mater* 2009; 117: 1–9.
5. Horcajada P, Rámila A, Férey G, et al. Influence of superficial organic modification of MCM-41 matrices on drug delivery rate. *Solid State Sci* 2006; 8: 1243–1249.

6. Airoldi C and Oliveira VV. Hydrophobic contribution to amoxicillin release associated with organofunctionalized mesoporous SBA-16 carriers. *Mater Res Bull* 2014; 59: 214–222.
7. Andrade GF, Soares DCF, Dos Santos RG, et al. Mesoporous silica SBA-16 nanoparticles: synthesis, physicochemical characterization, release profile, and in vitro cytocompatibility studies. *Micropor Mesopor Mater* 2013; 168: 102–110.
8. Vallet-Regi M. Nanostructured mesoporous silica matrices in nanomedicine. *J Intern Med* 2010; 267: 22–43.
9. Feliczak-Guzik A, Jadach B, Piotrowska H, et al. Synthesis and characterization of SBA-16 type mesoporous materials containing amine groups. *Micropor Mesopor Mater* 2016; 220: 231–238.
10. Feliczak-Guzik A, Wawrzynczak A and Nowak I. Studies on mesoporous niobosilicates synthesized using F127 triblock copolymer. *Adsorption* 2009; 15: 247–253.
11. Grudzien RM, Blitz JP, Pikus S, et al. Cage-like ordered mesoporous organosilicas with isocyanurate bridging groups: synthesis, template removal and structural properties. *Micropor Mesopor Mater* 2009; 118: 68–77.
12. Thomas MJK, Slipper I, Walunj A, et al. Inclusion of poorly soluble drugs in highly ordered mesoporous silica nanoparticles. *Int J Pharm* 2010; 387: 272–277.
13. Hu Y, Wang J, Zhi Z, et al. Facile synthesis of 3D cubic mesoporous silica microspheres with a controllable pore size and their application for improved delivery of a water-insoluble drug. *J Colloid Interface Sci* 2011; 363: 410–417.
14. Hu Y, Zhi Z, Zhao Q, et al. 3D cubic mesoporous silica microsphere as a carrier for poorly soluble drug carvedilol. *Micropor Mesopor Mater* 2012; 147: 94–101.
15. Lopes SM, Nogueira KAB, Gama MS, et al. Synthesis and characterization of ordered mesoporous silica (SBA-15 and SBA-16) for adsorption of biomolecules. *Micropor Mesopor Mater* 2013; 180: 284–292.
16. Zhu YF, Shi JL, Li YS, et al. Storage and release of ibuprofen drug molecules in hollow mesoporous silica spheres with modified pore surface. *Micropor Mesopor Mater* 2005; 85: 75–81.
17. Manzano M, Aina V, Areán CO, et al. Studies on MCM-41 mesoporous silica for drug delivery: effect of particle morphology and amine functionalization. *Chem Eng J* 2008; 137: 30–37.
18. Kamarudin NHN, Jalil AA, Triwahyono S, et al. Variation of the crystal growth of mesoporous silica nanoparticles and the evaluation to ibuprofen loading and release. *J Colloid Interface Sci* 2014; 421: 6–13.
19. Granero G, Longhi MR, Mora MJ, et al. Biowaiver monographs for immediate release solid oral dosage forms: furosemide. *J Pharm Sci* 2010; 99: 2544–2556.
20. Horcajada P, Rámila A, Pérez-Pariente J, et al. Influence of pore size of MCM-41 matrices on drug delivery rate. *Micropor Mesopor Mater* 2004; 68: 105–109.
21. Kruk M, Jaroniec M and Sayari A. Application of large pore MCM-41 molecular sieves to improve pore size analysis using nitrogen adsorption measurements. *Langmuir* 1997; 13: 6267–6273.
22. Qi F, Wu J, Fan Q-Z, et al. Preparation of uniform-sized exenatide-loaded PLGA microspheres as long-effective release system with high encapsulation efficiency and bio-stability. *Colloid Surface B* 2013; 112: 492–498.
23. European Pharmacopoeia Commission, Council of Europe. *European pharmacopoeia*. 8th ed. Strasbourg: European Directorate for the Quality of Medicines & Health Care, 2013.
24. Salonen J, Laitinen L, Kaukonen AM, et al. Mesoporous silicon microparticles for oral drug delivery: loading and release of five model drugs. *J Control Release* 2005; 108: 362–374.
25. Mesa M, Sierra L, Patarin J, et al. Morphology and porosity characteristics control of SBA-16 mesoporous silica. Effect of the triblock surfactant pluronic F127 degradation during the synthesis. *Solid State Sci* 2005; 7: 990–997.
26. Petushkov A, Yoon S and Larsen SC. Synthesis of hierarchical nanocrystalline ZSM-5 with controlled particle size and mesoporosity. *Micropor Mesopor Mater* 2011; 137: 92–100.
27. Grudzien RM, Grabicka EB and Jaroniec M. Adsorption studies of thermal stability of SBA-16 mesoporous silicas. *Appl Surf Sci* 2007; 253: 5660–5665.
28. Goscianska J, Olejnik A, Nowak I, et al. Ordered mesoporous silica modified with lanthanum for ibuprofen loading and release behaviour. *Eur J Pharm Biopharm* 2015; 94: 550–558.
29. Lehto VP, Vähä-Heikkilä K, Paski J, et al. Use of thermoanalytical methods in quantification of drug load in mesoporous silicon microparticles. *J Therm Anal Calorim* 2005; 80: 393–397.
30. Salonen J, Paski J, Vähä-Heikkilä K, et al. Determination of drug load in porous silicon microparticles by calorimetry. *Phys Stat Sol (A)* 2005; 202: 1629–1633.
31. Hirvonen J, Laaksonen T, Peltonen L, et al. Feasibility of silicon-based mesoporous materials for oral drug delivery applications. *Dosis* 2008; 24: 129–149.
32. Heikkilä T, Salonen J, Tuura J, et al. Evaluation of mesoporous TCPSi, MCM-41, SBA-15, and TUD-1 materials as API carriers for oral drug delivery. *Drug Deliv* 2007; 14: 337–347.
33. Thommes M, Kaneko K, Neimark AV, et al. Physisorption of gases, with special reference to the evaluation of surface area and pore size distribution (IUPAC Technical Report). *Pure Appl Chem* 2015; 87: 1051–1069.
34. Otsuka K, Wagner C, Selen A, et al. Prediction of in-vivo pharmacokinetic profile for immediate and modified release oral dosage forms of furosemide using an in-vitro–in-silico–in-vivo approach. *J Pharm Pharmacol* 2015; 67: 651–665.
35. Ambrogi V, Perioli L, Pagano C, et al. Use of SBA-15 for furosemide oral delivery enhancement. *Eur J Pharm Sci* 2012; 46: 43–48.

36. Lin CX, Qiao SZ, Yu CZ, et al. Periodic mesoporous silica and organosilica with controlled morphologies as carriers for drug release. *Micropor Mesopor Mater* 2009; 117: 213–219.
37. Izquierdo-Barba I, Martinez A, Doadrio AL, et al. Release evaluation of drugs from ordered three-dimensional silica structures. *Eur J Pharm Sci* 2005; 26: 365–373.
38. Ambrogi V, Perioli L, Pango C, et al. MCM-41 for furosemide dissolution improvement. *Micropor Mesopor Mater* 2012; 147: 343–349.
39. Díaz-Morales U, Bellussi G, Carati A, et al. Ethane-silica hybrid material with ordered hexagonal mesoporous structure. *Micropor Mesopor Mater* 2006; 87: 185–191.
40. Xia Y and Mokaya R. High surface area ethylene-bridged mesoporous and supermicroporous organosilica spheres. *Micropor Mesopor Mater* 2005; 86: 231–242.
41. Qu F, Zhu G, Lin H, et al. A controlled release of ibuprofen by systematically tailoring the morphology of mesoporous silica materials. *J Solid State Chem* 2006; 179: 2027–2035.
42. FDA. Waiver of in vivo bioavailability and bioequivalence studies for immediate-release solid oral dosage forms based on a biopharmaceutics classification system guidance for industry waiver of in vivo bioavailability and bioequivalence studies for immediate-R, 2015.
43. Heikkilä T, Salonen J, Tuura J, et al. Mesoporous silica material TUD-1 as a drug delivery system. *Int J Pharm* 2007; 331: 133–138.
44. Zhang Y, Huo M, Zhou J, et al. DDSolver: an add-in program for modeling and comparison of drug dissolution profiles. *AAPS J* 2010; 12: 263–271.
45. USP 38 – NF 33. *The United States Pharmacopeia and National Formulary 2015 main edition plus supplements 1 and 2*. Stuttgart: Deutscher Apotheker Verlag, 2015.
46. Tsume Y, Mudie DM, Langguth P, et al. The biopharmaceutics classification system: subclasses for in vivo predictive dissolution (IPD) methodology and IVIVC. *Eur J Pharm Sci* 2014; 57: 152–163.
47. Potthast H, Dressman JB, Juninger HE, et al. Biowaiver monographs for immediate release solid oral dosage forms: ibuprofen. *J Pharm Sci* 2005; 94: 2121–2131.
48. Refsgaard HFH, Jensen BF, Brockhoff PB, et al. In silico prediction of membrane permeability from calculated molecular parameters. *J Med Chem* 2005; 48: 805–811.
49. PhamThe H, Gonzalez-Ivarez I, Bermejo M, et al. In silico prediction of Caco-2 cell permeability by a classification QSAR approach. *Mol Inform* 2011; 30: 376–385.